Short Note

Time-Frequency Analysis of Explosions in the Ammunition Factory in Novaky, Slovakia

by Miriam Kristekova, Peter Moczo, Peter Labak, Andrej Cipciar, Lucia Fojtikova, Jan Madaras, and Jozef Kristek

Abstract A sequence of explosions occurred in an ammunition factory in Novaky, Slovakia, on 2 March 2007 and caused a major industrial accident. The origin times and number of explosions were key aspects for the state investigation team to explain the primary cause and development of the accident. An analysis of seismic records was the only way to determine reliable origin times. We were able to identify the two strongest explosions directly from the seismic records. Detailed time-frequency analysis enabled us to identify acoustic waves caused by the explosions. This led to the subsequent identification of two weaker explosions in seismic records and an indication of two even weaker explosions that could not be identified in the records. The seismic analysis is supported by results of the onsite investigation by the state investigation team.

Introduction

On 2 March 2007 just after 15:26 UTC (16:26 local time) a sequence of explosions occurred in an ammunition factory in Novaky, Slovakia (VOP Novaky). Eye witnesses reported two or three explosions within a few minutes (Fig. 1). The explosions destroyed the factory, killed eight people, and injured more than 30 people. They also caused damage in the neighboring area. Damage to building windows caused by the shock wave was reported at distances of more than 10 km. A state investigation team was charged with explaining the primary cause of the first explosion and the subsequent developments eventually leading to the major industrial accident. Obviously, the origin times and the number of explosions were the key facts for the investigation.

It was natural for seismologists to check the records of nearby seismic stations and to try to identify and locate the explosions. The analysis of seismic records was important to the investigation because, as was clear from the reports, no more accurate estimates of the origin times of the explosions could be found. The importance of the seismic analysis in the investigation of industrial explosions has been well demonstrated, for example, by Ichinose *et al.* (1999) and Koper *et al.* (2003).

Another important aspect of the event was that its origin, that is, its hypocenter, was well known. The seismic data were therefore a good test of the automatic earthquake location system used in the area.

Seismic Networks in the Region

The explosions were recorded by seismic stations of the Slovak National Network of Seismic Stations (Geophysical Institute, Slovak Academy of Sciences, Bratislava), the Local Network of the Mochovce Nuclear Power Plant (NPP), the Local Network of the Little Carpathians (Progseis, Trnava, around the Bohunice NPP), the Czech Regional Seismic Network (Geophysical Institute, Academy of Sciences of the Czech Republic, Prague, and Institute of Physics, Masaryk University, Brno), the Hungarian Seismological Network (Geodetic and Geophysical Research Institute, Hungarian Academy of Sciences, Budapest), the Austrian Seismological Network (Central Institute for Meteorology and Geodynamics [ZAMG], Vienna), and the Polish Seismological Network (Geophysical Institute, Polish Academy of Sciences, Warsaw).

The Slovak seismic stations *dlzi*, SMOL, LIKS, STHS, and KECS have 1 sec short-period seismometers Lennartz LE-3D lite, while KOLL has a 1 sec short-period seismometer Guralp CMG-40T. Broadband STS2 seismometers are located at VYHS and CRVS. The seismometers are three component. There are three one-component SKD seismometers at ZST.

Because the real-time exchange of waveforms exists in the region (Van Eck *et al.*, 2004; Labak *et al.*, 2008; also see the Data and Resources section), the strongest explosion was automatically located.

Figure 1. Amateur photograph of explosions in the VOP Novaky, Slovakia, on 2 March 2007 after 15:26 UTC.

Automatic and European–Mediterranean Seismological Centre Locations

The automatic locations for the strongest explosion were provided by the Geophysical Institute, Slovak Academy of Sciences, Bratislava (BRA), the Geophysical Institute, Academy of Sciences of the Czech Republic, Prague (GFU), and the European–Mediterranean Seismological Centre (EMSC). All three agencies used records from almost the same set of seismic stations (eight BRA, eight GFU, and nine EMSC, see the EMSC web site listed in the Data and Resources section for the relevant event). Seven stations in the distance range of 0.3°–1.4° from the hypocenter were used by all three agencies. Only *P*-wave onsets were used. BRA used International Association of Seismology and Physics of the Earth's Interior (IASPEI) 91 (Kennett, 1991) and LocSAT (Bratt and Bache, 1988; Bratt and Nagy, 1991). GFU used IASPEI 91 and grid search (Antelope). EMSC used the Jeffreys–Bullen and local models and Locgse (LDG, Paris). For the models and location procedures see also Godey *et al.* (2006) and Labak *et al.* (2008).

Automatic locations are listed in Table 1. The estimated epicenter coordinates do not differ more than 0.1°, which is the level of the round-off error. The distance between the true hypocenter and located hypocenters by BRA and EMSC is 5.7 km, which also is the level of the round-off error. Automatically estimated local magnitudes are close to the EMSC reporting threshold (2.0).

Analysis in the Time Domain

The SeismicHandler software package (Stammler, 1993) was used for the manual analysis of seismic records in the time domain. The two strongest explosions were identified on the records of the seismic stations (Fig. 2). Based on further analysis we will refer to these explosions as Ex3 and Ex4, explosion Ex4 being the automatically located event. Pg/Pn and Sg/Sn waves were interpreted and used for the locations. Ten stations with 17 phases were used for the location of Ex3, and 15 stations with 26 phases were used for the location of Ex4 (Fig. 3). The seismic stations were in the distance range of 0.06°–2.6°. We used the IASPEI 91 model for the LocSAT manual location. The estimated epicentral coordinates and origin times of Ex3 and Ex4 are shown in Table 2. The manual location of Ex4 is considerably more accurate than the automatic one—1 km compared to the 5.7 km distance between the true and located hypocenters. The distance between the true and located hypocenters for Ex3 is 0.6 km.

Time-Frequency Analysis

It was clear from the beginning that the seismic signals of the two strongest explosions could mask smaller explosions, and their identification in the time domain could be extremely difficult, if practically possible. Gibbons and Ringdal (2006) successfully combined array and cross-correlation analyses to detect weak similar colocated seismic events. Because of the geometrical configuration of the seismic stations from which records are available and the fact that we cannot assume very similar source mechanisms (eventually confirmed by the state investigation team), we cannot apply the same technique.

It was more likely to identify possible smaller explosions using time-frequency (TF) decompositions of the seismic records. This is because time-frequency analysis is an especially useful analyzing tool for complicated nonstationary signals in which spectral content changes considerably with time. Seismic phases and waves can often be identified by distinct time-frequency patterns and/or position in the time-frequency plane.

For the time-frequency decomposition of the seismic records, we used the continuous wavelet transform with the analyzing Morlet wavelet. The continuous wavelet transform (CWT) of signal $s(t)$ is defined by

Table 1
Automatic Locations of the Strongest Explosion (Ex4) According to the BRA, GFU, and EMSC Agencies

Origin Time (UTC)	Latitude (°N)	Longitude (°E)	Magnitude (M_L)	Region	Agency
15:28:07.0	48.7	18.5	2.1	Slovakia	BRA
15:28:05.3	48.7	18.6	2.3	Slovakia	GFU
15:28:04.9	48.7	18.5	2.2	Slovakia	EMSC
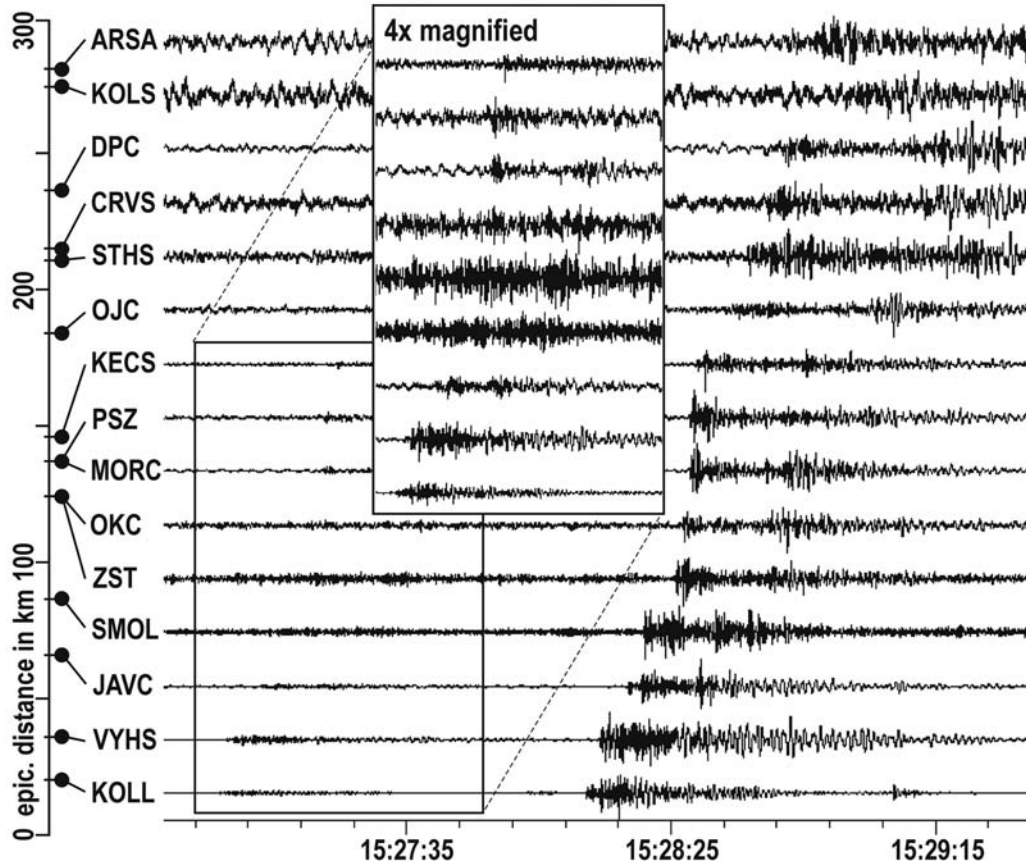
Figure 2. Vertical component of the ground velocity at 15 seismic stations. The strongest explosion (Ex4) is clearly visible. The second strongest explosion (Ex3) has considerably smaller amplitudes; therefore, this section of traces in the left-hand bottom rectangle is magnified. The vertical axis with black circles indicates epicentral distances of the seismic stations.

$$\mathrm{CWT}_{(a,b)}\{s(t)\} = \frac{1}{\sqrt{|a|}} \int_{-\infty}^{\infty} s(t) \psi^* \left(\frac{t-b}{a} \right) dt, \quad (1)$$

where t is time, a is the scale parameter, b is the translational parameter, and ψ is the analyzing wavelet. The asterisk denotes the complex conjugate function. The scale parameter a is inversely proportional to frequency f. A Morlet wavelet

$$\psi(t) = \pi^{-1/4} \exp(i\omega_0 t) \exp(-t^2/2) \quad (2)$$

with $\omega_0 = 6$ was used as the analyzing wavelet. The wavelet has zero amplitudes at negative frequencies—it is an analytical signal, also called the progressive wavelet. By choosing a relation between scale parameter a and frequency f in the form

$$a = \omega_0/2\pi f, \quad (3)$$

the time-frequency representation (TFR) of signal $s(t)$ can be defined as

$$\mathrm{TFR}(t, f) = \sqrt{\frac{2\pi|f|}{\omega_0}} \int_{-\infty}^{\infty} s(\tau) \psi^* \left(2\pi f \frac{\tau - t}{\omega_0} \right) d\tau. \quad (4)$$

A more detailed mathematical background on the continuous wavelet transform and Morlet wavelet can be found, for example, in monographs by Daubechies (1992) and Holschneider (1995). Kristekova (2006) and Kristekova *et al.* (2006) numerically demonstrated properties of the TFR defined here.

The software package SEIS-TFA (2006) developed by Kristekova (2006) was used for computation of the TFR of all three components of the recorded motion.

Looking at the TFR of the KOLL seismic record of Ex3 (Fig. 4, left-hand panel), we can recognize two specific TFR patterns at later times—they are marked by ellipses. The acoustic speed in dry air at a temperature of 8°C (in the Novaky area in the afternoon in March) was approximately 337 m/sec. The arrival time of the acoustic wave due to Ex3 at the seismic station KOLL (distance to VOP Novaky is 21 km) should be equal to 15:27:57.1 UTC ± 1 sec. In fact, the second TFR pattern, marked by the cyan ellipse in Figure 4, corresponds to this estimated arrival time. In the TFR of the KOLL record of Ex4 (Fig. 4, right-hand panel), we recognize a very similar pattern to those seen in the TFR of Ex3. The pattern is marked by the dark green ellipse. Its arrival time corresponds to the arrival time estimated for the acoustic wave due to Ex4.
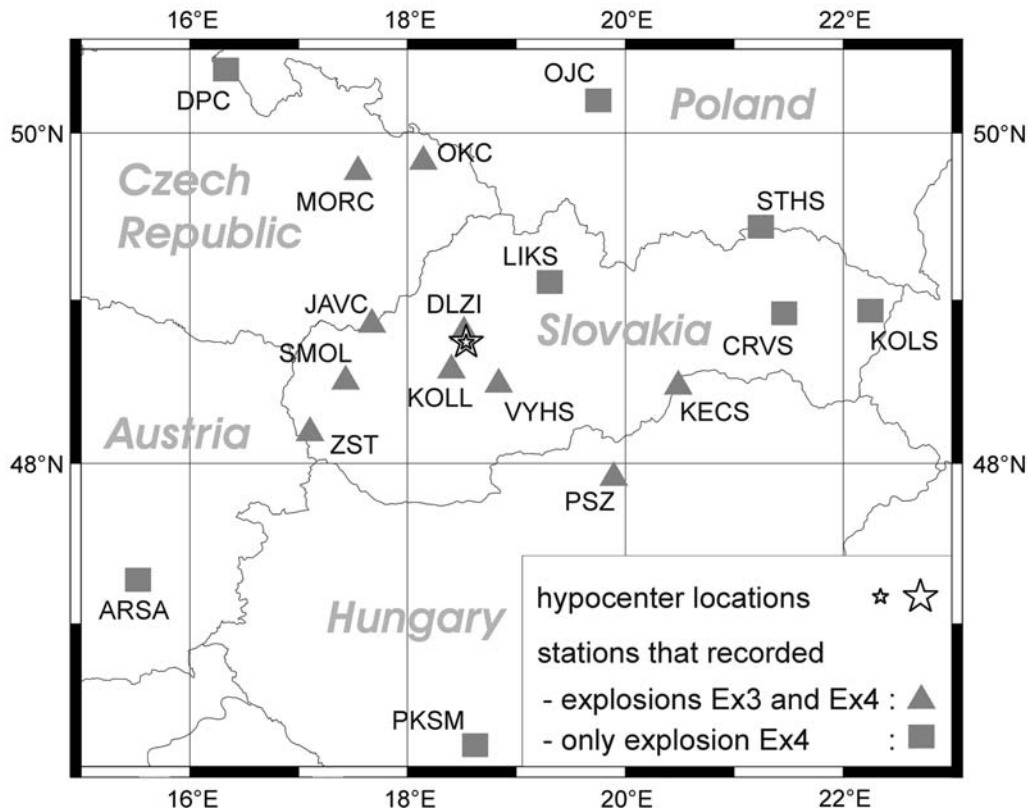
Figure 3.   Hypocenters of the two largest explosions, Ex3 and Ex4, and the seismic stations that recorded the explosions.

The fact that the seismic waves at KOLL from both clearly located and identified explosions are followed by very similar TFR patterns arriving at times estimated for the acoustic waves led us to check arrival times of the suspected acoustic waves and those of the *P* and *S* waves due to Ex3 and Ex4 at other seismic stations. The travel times and results of the linear regressions are shown in Figure 5. The estimated apparent velocities for the *P* and *S* waves correspond well to those in our velocity model. The TF analysis and the third estimated apparent velocity (341 ± 1 m/sec) led us to the conclusion that the two later arrivals with the specific TFR patterns correspond to the acoustic waves from explosions Ex3 and Ex4.

We can also note that the signatures in the ground-velocity records of the acoustic waves at station *dlzi* (starting at 15:27:16.6 UTC for Ex3 and 15:28:25.9 UTC for Ex4, see the right-hand panel of Fig. 6) are very similar to those found

by Kanamori *et al.* (1991) and Cates and Sturtevant (2002) for the acoustic shock *N* wave. This supports the interpretation that the analyzed arrivals at station *dlzi* correspond to the direct acoustic shock waves.

As we already mentioned, in the TFR of Ex3 at station KOLL (Fig. 4, left-hand panel), we can also recognize a very similar specific pattern at approximately 15:27:26 UTC, overlapping with the coda of seismic waves of Ex3. The pattern is marked by the orange ellipse. Because such an earlier pattern is not present in the otherwise very similar TFR of Ex4 (Fig. 4, right-hand panel), it is likely that it is not a part of the coda of Ex3. Based on the similarity of the TFR patterns marked by the cyan, green, and orange ellipses, we can consider that the pattern marked by the orange ellipse possibly also represents an acoustic wave. The left-hand column in Figure 7 shows the particle motion of the corresponding wave group. The particle motion clearly agrees with the po-

Table 2

Parameters of Four Identified Explosions

Explosion Number	Origin Time (UTC)	Latitude (°N)	Longitude (°E)	Magnitude (M_L)	Automatic Location	Manual Location	Time-Frequency Analysis
Ex1	15:26:24 ± 2 sec	48.86[*]	18.56[*]	—	No	Yes[*]	Yes
Ex2	15:26:53.8 ± 1 sec	—	—	—	No	No	Yes
Ex3	15:26:55.4 ± 1 sec	48.74	18.54	0.6	No	Yes	Yes
Ex4	15:28:05.3 ± 1 sec	48.75	18.55	2.1	Yes	Yes	Yes

[*]Location is based on four phases only.
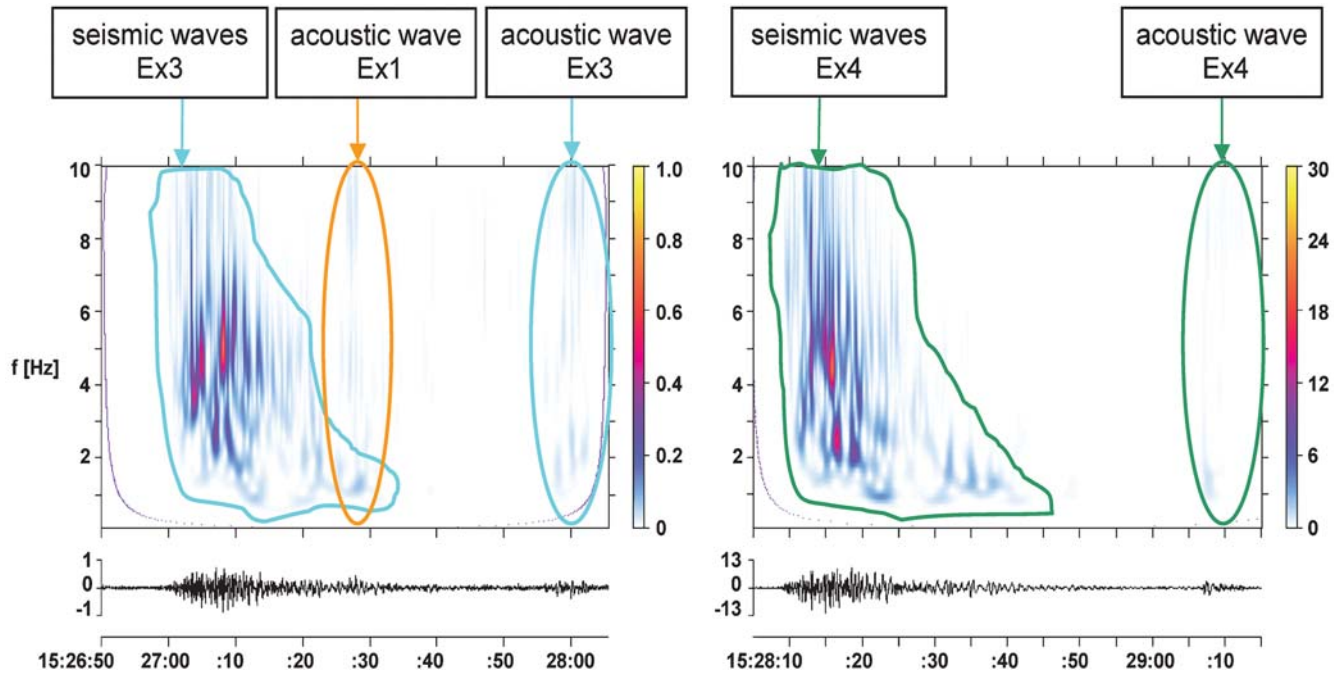
Figure 4. Records of the radial component at the seismic station KOLL for Ex3 (left-hand panel) and Ex4 (right-hand panel), and their time-frequency representations (TFRs). Patterns of TFR corresponding to the acoustic waves are marked by ellipses. Amplitudes are normalized, with 1 corresponding to the maximum amplitude of Ex3.

sition of the epicenter and with the oblique incidence from the atmosphere onto the surface. If, therefore, the arrival should correspond to the acoustic wave, it is clear that it is not due to Ex3. Considering the same hypocenter location and propagation velocity, the difference in the arrival times of the two TFR patterns (cyan and orange), 31.5 ± 1 sec, should also correspond to the difference of the origin times of Ex3 and some other earlier explosion that could cause the

Figure 5. Stars, squares, and circles represent travel times of the arrivals identified in seismograms (Ex3, Ex4) and TFRs (Ex2) for stations *dlzi*, KOLL, VYHS, JAVC, and SMOL. Straight lines represent the results of the linear regressions for the *P*, *S*, and acoustic waves.

earlier (orange) TFR pattern. The estimated origin time of the earlier smaller explosion should be then 15:26:23.9 UTC. Consequently, *P* waves corresponding to this explosion should arrive at seismic stations also 31.5 ± 1 sec earlier than the *P* waves of Ex3.

A posteriori detailed inspection of seismic records within the corresponding time window did reveal onsets of seismic phases of the possible weaker explosion (Fig. 8). The use of the four identified seismic phases to locate the event, hereafter referred to as Ex1, gave the location shown in Table 2. Given just the four phases, the location is surprisingly good. Given the geometrical configuration of the stations, the accuracy is better in longitude than in latitude. The distance between the true and estimated hypocenter locations is 12.6 km. Based on the preceding arguments, we consider this event, Ex1, a weaker explosion. Obviously, due to the low signal-to-noise ratio, it was impossible to estimate M_L. Let us emphasize that without the indication from the TFR the visual inspection itself could hardly reveal the onset phases of Ex1.

The TFRs of Ex1, Ex3, and Ex4 enabled us to estimate ratios of the energy maxima of the acoustic waves to the energy maxima of the seismic waves. The ratios were considerably smaller for Ex3 and Ex4 compared to that for Ex1. Likely this can be considered an indication that the mechanism or source conditions of Ex1 were different from those of Ex3 and Ex4. For example, a weaker contact of the explosive with the ground or building in the case of Ex1 or another type of explosive could cause a relatively larger
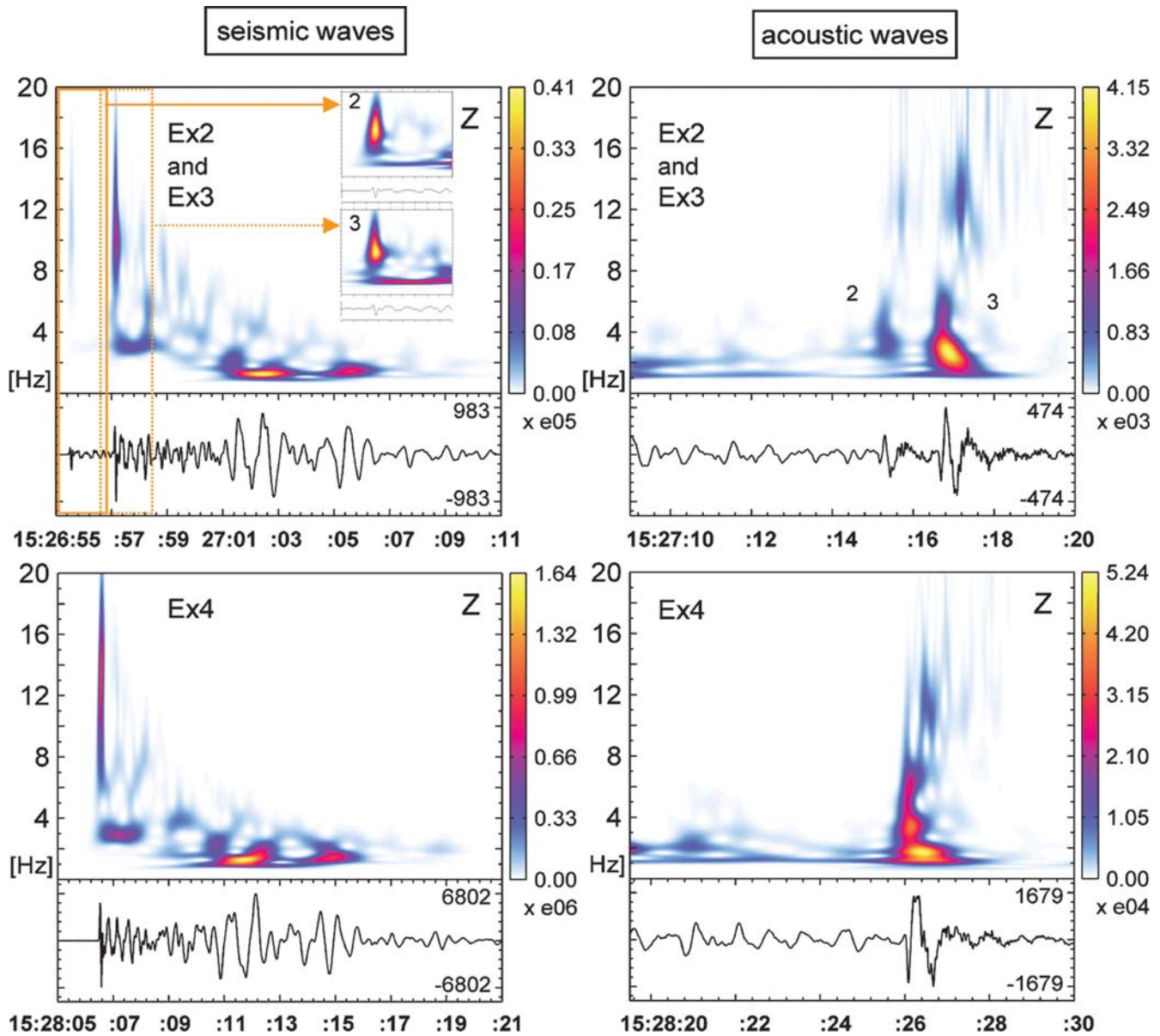
Figure 6. Records of the vertical (Z) velocity component at station *dlzi* and their TFRs for Ex2 and Ex3 (upper panel) and for Ex4 (lower panel). Left-hand panel: main seismic phases; right-hand panel: acoustic waves. The insets in the left-hand upper panel show detailed pictures of the *P* waves. The seismograms and TFRs in the insets are amplified relative to the main panel and scaled to their maximum values.

amount of energy to be released in the form of the acoustic wave. In fact, a difference in the source conditions was independently confirmed by the state investigation team. The team characterized Ex1 as an explosive deflagration (which releases much more energy into the atmosphere) and characterized Ex3 and Ex4 as detonations.

Figure 6, top panel, shows a seismic record with Ex3 at station *dlzi* and the corresponding TFR. We can clearly see the identified *P*-wave onset of Ex3 at 15:26:57 UTC. At approximately 15:26:55.4 UTC, that is, 1.6 sec earlier, we can recognize a smaller but similar onset. The TFR patterns corresponding to the two onsets are very similar, though with different amplitudes. The inserts in the left-hand panel show

detailed and amplified phases and corresponding TFRs. The similarity of the detailed amplified TFRs is striking. We therefore consider the earlier onset to be a possible *P*-wave onset of some weaker explosion. This idea is considerably supported by the analysis of the later part of the record with an already identified acoustic wave due to Ex3. A more detailed time scale enables us to clearly distinguish two arrivals with similar shapes both in the time domain and TFR. The weaker wave arrives just 1.6 sec prior to the acoustic wave created by Ex3.

For comparison we show in the bottom panel of Figure 6 a record section for Ex4. The bottom panel exhibits seismic and acoustic waves of Ex4 similar to those of Ex3. At the
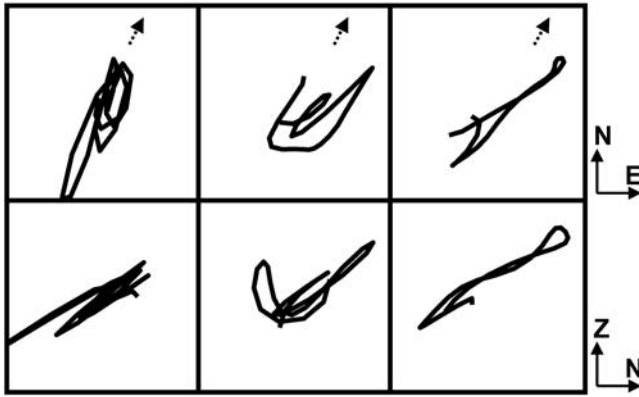
Figure 7. Particle motions of the acoustic waves at station KOLL. Left-hand column: Motions due to Ex1; time window 15:27:26.20–15:27:26.50 UTC. Central and right-hand columns: motions probably due to weaker explosions; time windows 15:27:33.00–15:27:33.35 UTC and 15:27:38.25–15:27:38.55 UTC. Top panel: particle motion in the horizontal northeast plane. Bottom panel: particle motion in the vertical Z-north plane. Arrows indicate the direction to the epicenter. Amplitudes for the two probable weaker explosions are amplified 2.5 times compared to those for Ex1.

same time we do not see in the bottom panel anything like the earlier weak arrivals in the top panel. A weaker arrival, 1.6 sec prior to the acoustic wave of Ex3, can be also seen in the KOLL record and its TFR in Figure 9. We conclude that the weaker arrivals are seismic and acoustic phases

due to some smaller explosion with the origin time equal to 15:26:53.8 UTC ± 1 sec. We label this event as Ex2.

Similarities of the TFRs of Ex2 and those of Ex3 and Ex4 indicate that mechanisms and/or origin conditions of explosions Ex2, Ex3, and Ex4 were similar. The difference is in the low-frequency content of the acoustic waves: the acoustic wave of Ex2 lacks energy below 2 Hz compared to Ex3 and Ex4.

A detailed TFR of a later part of the KOLL record of Ex3 with the acoustic wave due to Ex1 displays two more patterns that could possibly represent weaker acoustic waves—see Figure 10. Their particle motions are shown in Figure 7 (central and right-hand columns). Although their amplitudes are very weak, it is possible to see good agreement with the direction to the epicenter. We computed the ratios of the average TFR values in the yellow regions (corresponding to the tentative acoustic waves, Fig. 10) to the average TFR values outside the regions (noise). The ratios 4.2 for the first tentative acoustic wave and 3.1 for the second acoustic wave also indicate the presence of signals buried in the noise (with the signal energy only slightly higher than that of the noise). Because of the low signal-to-noise ratio we were unable to identify corresponding seismic phases. It is also possible that they correspond to events that released most of or all of the energy into the atmosphere. Such a case was reported, for example, in the analysis of seismic records of a missile silo explosion by Johnston (1987).
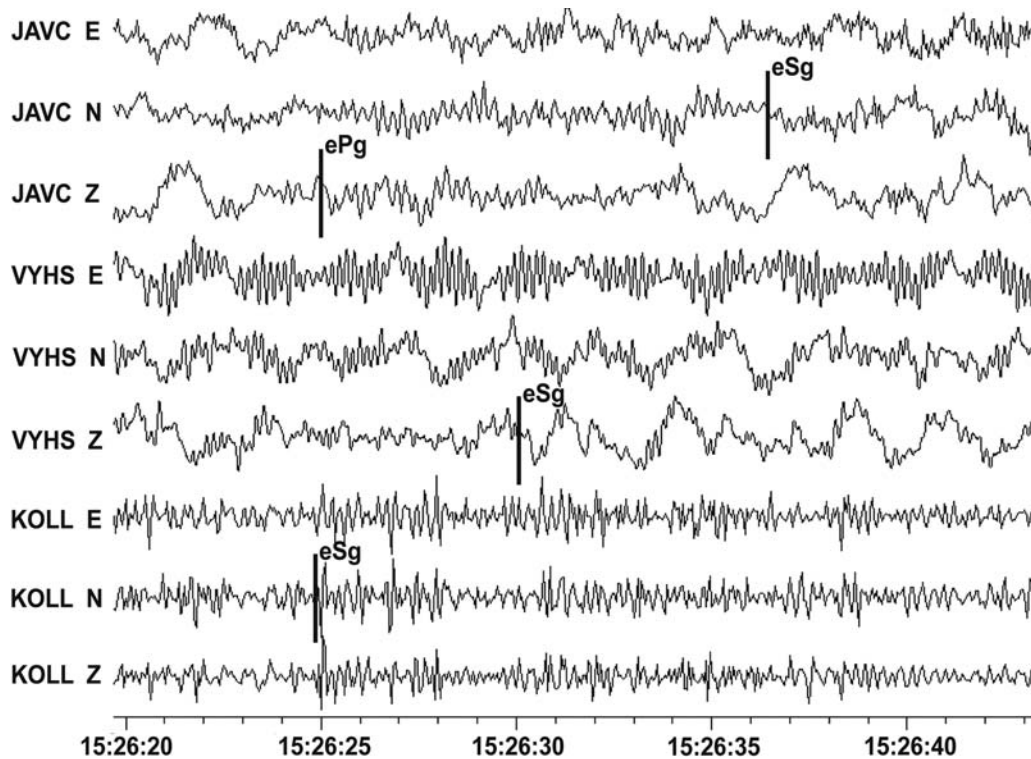
Figure 8. Seismic records of the ground velocity (Z, north–south, east–west) recorded at stations KOLL, VYHS, and JAVC. Vertical bars indicate arrival times of the identified seismic phases for Ex1.
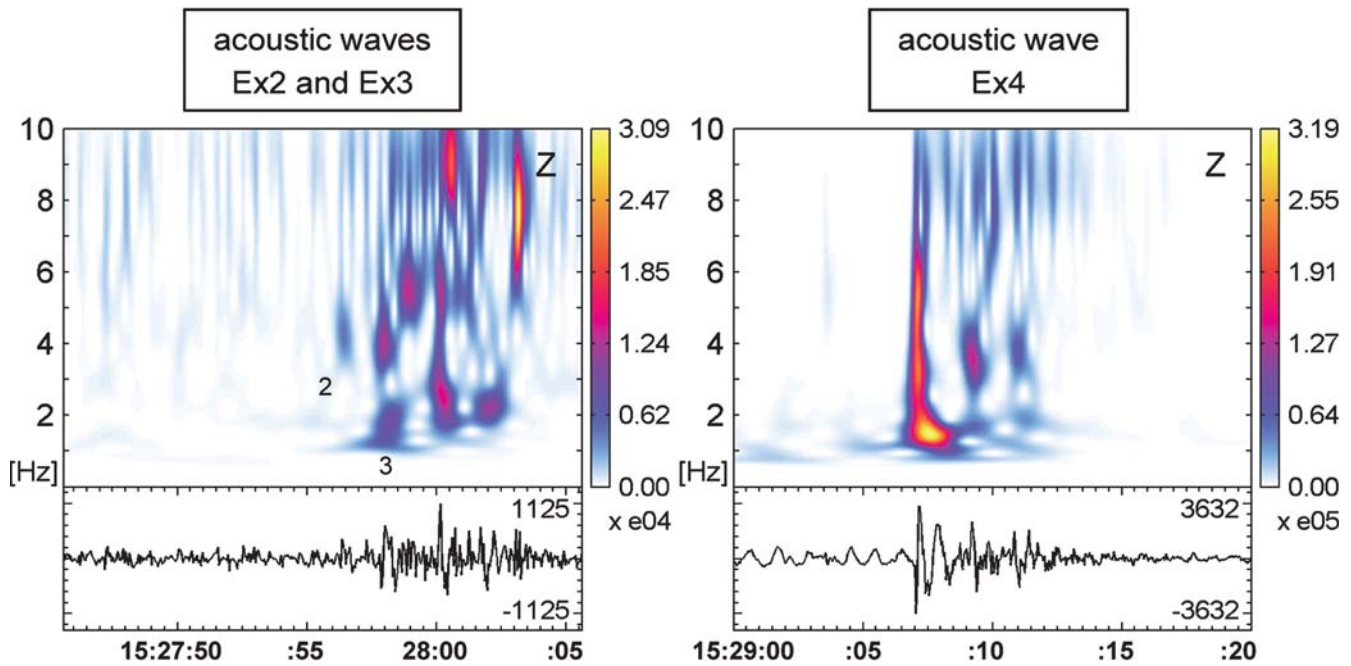
Figure 9. Records of the vertical (Z) ground velocity of the acoustic waves at station KOLL and their TFRs for Ex2, Ex3, and Ex4.

Discussion and Conclusions

Only the strongest of the explosions (see Table 2), Ex4 with $M_{L(BRA)}$ 2.1, was automatically located by the BRA, GFU, and EMSC agencies. The automatic location by BRA used eight automatic picks. Only two picks were available in the automatic system of BRA for Ex3, with $M_{L(BRA)}$ 0.6, and did not allow an automatic location. We can speculate that the threshold size of an event that can be automatically located by BRA lies somewhere between Ex3 and Ex4, likely closer to Ex4.

Although the magnitude of Ex4 is close to the EMSC reporting threshold (2.0), the automatic locations of Ex4 by the BRA, GFU, and EMSC agencies were very accurate—the distances between the true hypocenter and its automatic locations are at the level of round-off error. The manual location made use of the identified phases (including S waves) from a larger number of stations and considerably improved the accuracy of the location—the distance between the true hypocenter and its location decreased from 5.7 km (automatic) down to 1 km (manual).

The TFR of the seismic records enabled us to identify specific TFR patterns that were afterwards interpreted as acoustic waves caused by two weaker explosions (Ex1 and Ex2) that we were originally unable to notice in the seismic records themselves due to the low signal-to-noise ratio and partial overlapping of the records. The TFR also led us to determine that the mechanism or source conditions of Ex1 were different from those of the other explosions, mainly Ex3 and Ex4. Ex1 produced a relatively stronger acoustic wave. Moreover, the detailed TFR led to the indication of

another two weaker explosions with timing between Ex1 and Ex2.

Our results are supported by onsite investigations based directly on crater locations, distribution of explosives, and other available facts. Figure 11 shows a photograph of the area. Ex1 was the first initialization explosion. The crater was found after removal of debris and is shown in the insert. The conditions and type of explosives were different from those in the later explosions. Ex1, inside a building, caused a fire that then spread through halls and corridors and initiated later explosions of the explosives stored at different sites. The sites of craters and estimated scenario are consistent with timing found by our analysis of seismic records. The state investigation team also acknowledged the two indicated weakest (not labeled in this article) explosions based on the distribution of explosives.

This case study indicates that the time-frequency analysis can help considerably in the interpretation of seismic records and the identification of explosions. In this case the determined hypocentral times of the explosions are the only reliable times the state investigation team could use.

Data and Resources

Seismograms used in this study come from the Virtual Regional Seismic Network of the Geophysical Institute, Slovak Academy of Sciences. Data can be obtained from www.seismology.sk and www.seismology.sk/Regional_Network/regional_network_A.html (last accessed July 2008). Data from the seismic station *dlzi* were provided by ProgSeis Company and are proprietary. They cannot be released to the public. Automatic locations of the strongest explosion
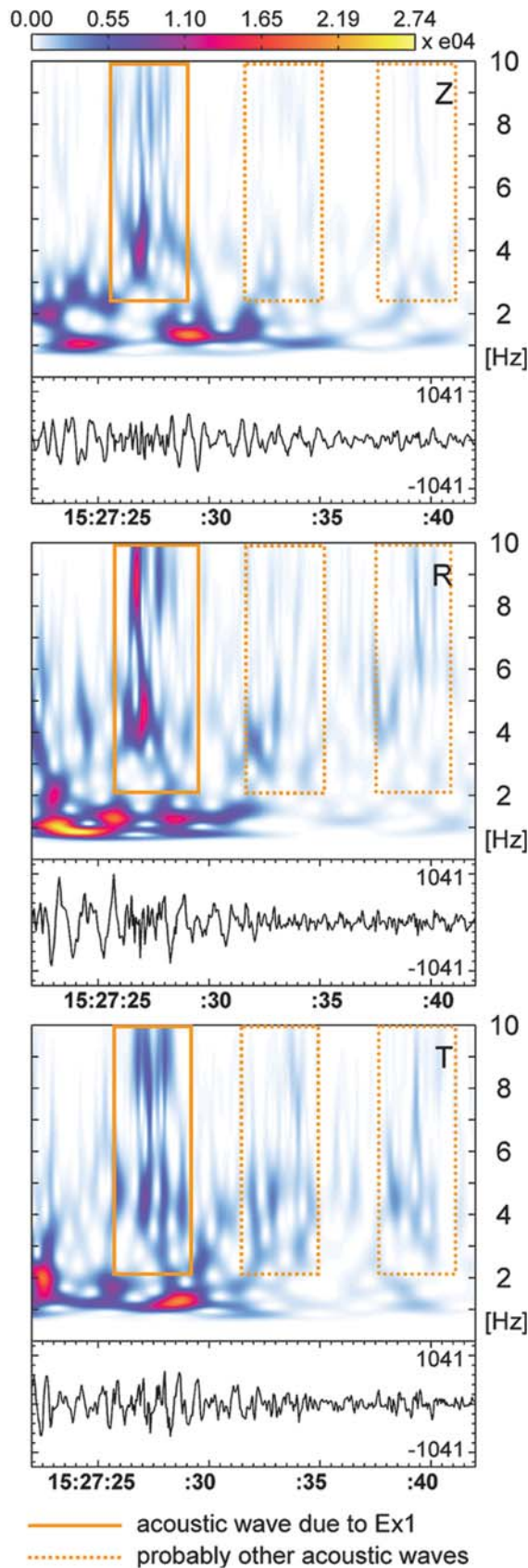
Figure 10. Records of the vertical (*Z*), radial (*R*), and transverse (*T*) velocity components of the acoustic waves at station KOLL and their TFRs.
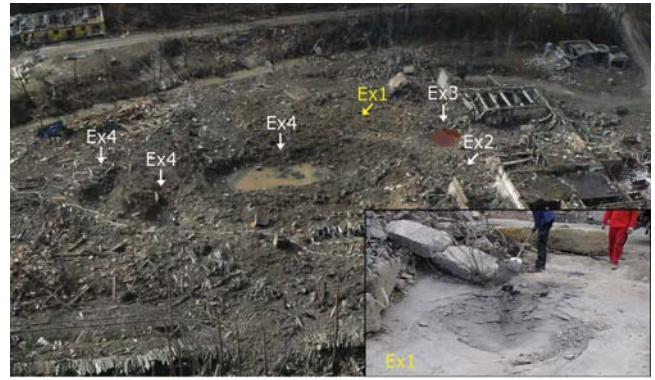
Figure 11. Identified craters. The site of explosion Ex1 (shown in the inset) was uncovered by the investigators after the main photograph had been taken. Similarly, the site of explosion Ex2 was uncovered afterwards. Explosion 4 was most likely due to stored explosives at three sites indicated by the Ex4 label. The sites of the two (unnamed) weakest explosions are not shown here. Investigators acknowledged two explosions due to small storages of explosives in the space between the site of Ex1 and the largest crater of Ex4. The latter crater measured 34 m (length) by 21 m (width) by 7 m (depth).

(Ex4) were taken from the European–Mediterranean Seismological Centre (EMSC) at www.emsc-csem.org (last accessed July 2008).

Acknowledgments

References

Bratt, S., and T. C. Bache (1988). Locating events with a sparse network of regional arrays, *Bull. Seismol. Soc. Am.* **78,** 780–798.

Bratt, S., and W. Nagy (1991). The LocSAT program, Science Applications International Corporation, San Diego.

Cates, J. E., and B. Sturtevant (2002). Seismic detection of sonic booms, *J. Acoust. Soc. Am.* **111,** 614–628.

Daubechies, I. (1992). *Ten Lectures on Wavelets*, Society for Industrial and Applied Mathematics, Philadelphia.

Gibbons, S. J., and F. Ringdal (2006). The detection of low magnitude seismic events using array-based waveform correlation, *Geophys. J. Int.* **165,** 149–166.

Godey, S., R. Bossu, J. Guilbert, and G. Mazet-Roux (2006). The Euro-Mediterranean bulletin: a comprehensive seismological bulletin at regional scale, *Seism. Res. Lett.* **77,** 460–474.

Holschneider, M. (1995). *Wavelets: An Analysis Tool*, Clarendon Press, Oxford.

Ichinose, G. A., K. D. Smith, and J. G. Anderson (1999). Seismic analysis of the 7 January 1998 chemical plant explosion at Kean Canyon, Nevada, *Bull. Seismol. Soc. Am.* **89,** 938–945.

Johnston, A. C. (1987). Air blast recognition and location using regional seismograph networks, *Bull. Seismol. Soc. Am.* **77,** 1446–1456.

Kanamori, H., J. Mori, D. L. Anderson, and T. H. Heaton (1991). Seismic excitation by space shuttle Columbia, *Nature* **349,** 781–782.

Kennett, B. L. N. (1991). IASPEI 1991 seismological tables, Research School of Earth Sciences, Australian National University.

Koper, K. D., T. C. Wallace, and R. C. Aster (2003). Seismic recordings of the Carlsbad, New Mexico, pipeline explosion of 19 August 2000, *Bull. Seismol. Soc. Am.* **93,** 1427–1432.

Kristekova, M. (2006). Time-frequency analysis of seismic signals, *Ph.D. Thesis*, Geophysical Institute of the Slovak Academy of Sciences, Bratislava (in Slovak).

Kristekova, M., J. Kristek, P. Moczo, and S. M. Day (2006). Misfit criteria for quantitative comparison of seismograms, *Bull. Seismol. Soc. Am.* **96,** 1836–1850.

Labak, P., A. Cipciar, and M. Kristekova (2008). Monitoring of earthquakes on the territory of Slovak Republic by the National Network of the Seismic Stations in the period 2001–2005, *Slovak Geol. Mag.* (in press)

SEIS-TFA (2006). SEIS-TFA, the source code in Fortran 95, executable modules for seven TF analysis methods, and the users' guide are available from NuQuake, Bratislava, Slovak Republic, www.nuquake.eu (last accessed July 2008).

Stammler, K. (1993). Seismic Handler—programmable multichannel data handler for interactive and automatic processing of seismological analyses, *Comput. Geosci.* **19,** 135–140.

Van Eck, T., C. Trabant, B. Dost, W. Hanka, and D. Giardini (2004). Setting up a virtual broadband seismograph network across Europe, *EOS* **85,** no. **13**, 125–129.

Geophysical Institute
Slovak Academy of Sciences
Dubravska cesta 9
845 28 Bratislava 45, Slovak Republic
    (M.K., P.L., A.C., L.F., J.M.)

Faculty of Mathematics, Physics and Informatics
Comenius University
Mlynska dolina F1
842 48 Bratislava, Slovak Republic
    (P.M., J.K.)